

---

# Image Animation with Keypoint Mask

---

Or Toledano<sup>1</sup> Yanir Marmor<sup>1</sup> Dov Gertz<sup>1</sup>

**Table 1. Motion transfer example:** Given a YouTube clip of a Thai-Chi artist (top), and an image of another one, our method transfers the one’s performance onto the other (bottom).



## Abstract

Motion transfer is the task of synthesizing future video frames of a single source image according to the motion from a given driving video. This task is challenging due to the complexity of motion representation and the unknown relations between the driving video and the source image. Despite this difficulty, this problem attracted great interests from researches at the recent years, with gradual improvements. The problem can be thought as decoupling of motion and appearance, which is often solved by extracting the motion from keypoint movement. We chose to tackle the generic, unsupervised setting, where we need to apply animation to any arbitrary object, without any domain specific model for the structure of the input. In this work, we extract the structure from a keypoint heatmap, without an explicit motion representation. Then, the structures from the image and the video are extracted to warp the image according to the video, by a deep generator.

## 1. Introduction

Take a look at Figure 1 for two video sequences. The input is a YouTube clip of a Thai-Chi artist (the driving subject) performing a series of complex motions in the top

<sup>1</sup>Tel Aviv University. Correspondence to: Or Toledano <ortoledano@protonmail.com>, Yanir Marmor <yanirmr@gmail.com>, Dov Gertz <dovgertz1@gmail.com>.

row. Our algorithm’s output is shown in the bottom row. It refers to frames that appear to show a different person (the source subject) executing the same motions. The twist is that the source individual has never performed the same exact sequence of motions as the driver video. In reality, he was photographed doing another movement with no clear reference to the driving’s actions. And, as the figure shows, the source and the driving are of different appearances, have different backgrounds, and are dressed differently.

In this study, we propose a simple, however surprisingly efficient approach to the general motion transfer problem, which can be applied to any domain, similarly to (Siarohin et al., 2019): Given a source image of a person with the wanted appearance, and a driving video with the wanted structure/geometry, we synthesize a video by applying a deep motion generator per-frame. We assist the generator by feeding it with compact structural representations of the source and each frame of the driving video. That way, we obtain the target of a video of the source appearance and the driving motion, given any domain.

Researchers of some notable works (Section 2) observe that keypoint-based pose preserves motion signatures over time, while abstracting subject identities. We therefore use the keypoint-based pattern without any other motion priors. We obtain the keypoints and use them to animate images in a way that doesn’t need any external information about the subject or any assumption or prior about the scene.

Our contribution is twofold: first, we demonstrate that removing the motion prior will function and provide better accuracy outcomes, and second, we provide a compact representation with improved efficiency.

## 2. Related Work:

Motion transfer has gained a lot of coverage over the last twenty years. Early approaches based on manipulating existing video footage to generate new content. These included searching for frames in which the body position corresponds to a desired motion and using them to generate a new content (Bregler et al., 1997). Our approach is equally designed for videos, but rather than manipulating existing images, we learn to synthesize new movements that were never seen before with the new identities.

A number of techniques are based on calibrated multi camera systems to scan a target player and use an adapted 3D model of the target to control their motion in a new frame(Cheung et al., 2004). Our solution instead examines the transition of movement between 2D video subjects and prevents data calibration or 3D space information.

Latest approaches concentrate on the disentangling of appearance and activity and synthesizing of new motion videos (Tulyakov et al., 2018). Similarly, we apply our representation of motion to different target subjects to generate new motions. However, In contrast to these works, we did not use GAN but an encoder-decoder approach.

In comparison to the pixel-based approaches for image animation that were common until recently, keypoint-based approaches are now thought to have the ability to achieve high performance in the field of video reanimation. Some notable works in this area are (Siarohin et al., 2020), (Siarohin et al., 2019), (Kim et al., 2019), (Balakrishnan et al., 2018), (Ma et al., 2017), (Reed et al., 2017), (?).

Our work does not depend on a strong motion prior directly, but rather on a structure mask derived from a keypoint detector of a motion-based model, such as (Siarohin et al., 2020). The idea of using drawn keypoints as a geometry representation (structural mask) was already used in image-to-image translation works such as TransGaGa (Wu et al., 2019), in addition to some of the video reanimation works mentioned earlier.

The concept of using a structural mask in the context of image animation is demonstrated in (Shalev & Wolf, 2020). However, the current work differs by basing the mask off a motion related keypoint module, which saves us the hassle of perturbing the input hoping to achieve an identity-less mask which might not even be optimal. That way, we can base more of the motion representation on the deep network, reduce our prior, and leave some space for our network to optimize more. We also purpose an heatmap mask, which differs from some of the drawn keypoint masks mentioned.

### 3. Methodology

The network can be divided into two parts: obtaining the mask, and generating the synthesized frame. The generator architecture is constant amongst all of our variations, and can be described as low resolution generation from the source image, source mask and driving mask; Followed by up-scaling of the low scale synthesized prediction by passing it with the source frame to a high resolution generator. We created two different versions for the mask generator: the first, an absolute motion transfer; the second, a relative motion transfer. We chose to present the results for the first, absolute one, due to its performance. The performance drop for our second, relative version was expected because the

mask contained less structural information. The first version is referred as a "keypoint heatmap," while the second is referred as a "circles mask" or "keypoints after softmax".

#### 3.1. First mask version for absolute motion transfer, with warping

Our main mask for the project is obtained from carefully observing the keypoint module from (Siarohin et al., 2020). U-Net based keypoint modules of this form, work by extracting features, which pass through a *conv* layer to form a heatmap image  $K$  channels, where  $K$  is the number of keypoints. Then, a softmax is performed over the channels, and keypoints are extracted from the mean location of each heatmap channel. By carefully debugging the code, and the expectation for a segmentation map out of U-Net, we obtain Figure 1.

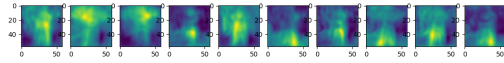


Figure 1.  $K$  channels of the keypoint detector network used in (Siarohin et al., 2020), before the softmax activation. Our main motion prior in this project.

Summing over the channels, we get Figure 2.

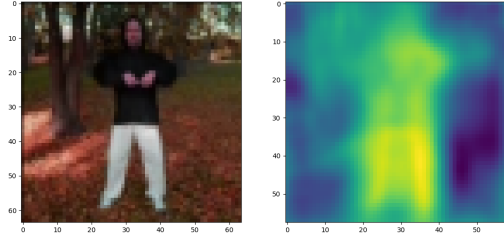


Figure 2. The sum of the  $K$  channels which is fed as a structural mask into the generator.

which is our output mask, aka the heatmap, pre softmax mask.

### 3.2. Second mask version for relative motion transfer

We purposes an additional "circles" only mask which can be used in the context of relative motion transfer during animation, as in (Siarohin et al., 2020), which isn't possible with the previous heatmap mask. The mask captures the image's geometry representation (Wu et al., 2019), and by requiring it to be represented as keypoints with a center, we can use the relative coordinates for the animation. This module, though, did not do as well as our heatmap mask module (Table 4).

While relative motion transition is not always desired, this work shows that a keypoint-only-prior-based module is feasible for the task. Since the only information contained in the pair of masks is the keypoint displacement, our deep network can only attempt to approximate a zero order approximation, we can anticipate results that are more close to (Siarohin et al., 2019).

By taking the softmax over the heatmap, we get Table 3.

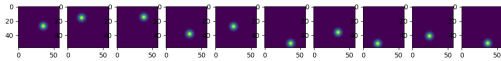


Figure 3.  $K$  channels of the keypoint detector network used in (Siarohin et al., 2020), after the softmax activation and Gaussian fit.

Summing over the channels, we get Table 4.

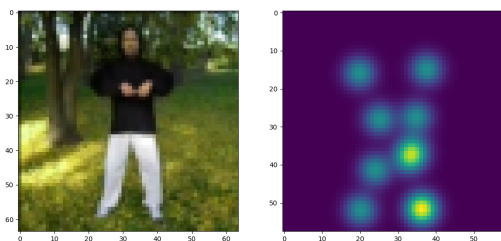


Figure 4. The sum of the  $K$  channels which is fed as a structural mask into the generator.

which is our output mask, aka the keypoints after softmax

mask.

### 3.3. Architecture

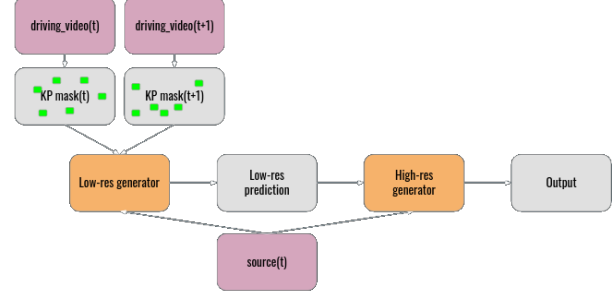


Figure 5. Architecture of the model. The keypoint mask can be either a keypoint heatmap such as in Figure 2, or drawn keypoint circles as in Figure 4.

Our architecture follows (Siarohin et al., 2020) without the dense motion module, after changing its keypoint generation module to return our mask. After the mask is obtained, we follow the encoder decoder approach as (Shalev & Wolf, 2020). Namely, the encoder of the low resolution generator consists of  $conv_{7 \times 7}$ ,  $batch\_norm$ ,  $relu$ , followed by six residual blocks of  $batch\_norm$ ,  $relu$ ,  $conv_{3 \times 3}$ ,  $batch\_norm$ ,  $relu$ ,  $conv_{3 \times 3}$ , (and a sum with the source). The residual blocks help to maintain the identity of the source image (He et al., 2015). The decoder consists of two blocks, each is a sequence of  $up\_sample_{2 \times 2}$ ,  $batch\_norm$ ,  $relu$ . The decoder is followed by a  $conv_{7 \times 7}$  and a  $sigmoid$  activation. For the high resolution generator, use an encoder (decoder) with five encoding (decoding) blocks, where each block is a sequence of  $conv_{3 \times 3}$ ,  $batch\_norm$ ,  $relu$   $avg\_pool_{2 \times 2}$ , and each decoding block is a sequence of  $up\_sample_{2 \times 2}$ ,  $conv_{3 \times 3}$ ,  $batch\_norm$ ,  $relu$ . We add skip connections from each of the encoding layers to its corresponding encoding layer, to form a U-Net architecture (Ronneberger et al., 2015).

### 3.4. Losses

We use the same perceptual loss as in (Siarohin et al., 2020) which is based on the implementation of (Wang et al., 2018). With the input driving frame  $D$  and the corresponding reconstructed frame  $\hat{D}$ , the reconstruction loss is written as:  $L_{rec}(\hat{D}, D) = \sum_{i=1}^I |N_i(\hat{D}) - N_i(D)|$ , where  $N_i(\cdot)$  is the  $i^{th}$  channel feature extracted from a specific VGG-19 layer (Simonyan & Zisserman, 2015) and  $I$  is the number of feature channels in this layer. Additionally we use this lose on a number of resolutions, forming a pyramid obtained by down-sampling  $\hat{D}$  and  $D$ , similarly to  $(\cdot), (\cdot)$ . The resolutions

Table 2. Images comparison

SOURCE IMAGE	DRIVING
X2FACE	
MONKEY-NET	
FOMM	
PERTURBED MASK	
OURS	

are  $256 \times 256$ ,  $128 \times 128$ ,  $64 \times 64$  and  $32 \times 32$ .

## 4. Experiments

### 4.1. Datasets

The Tai-chi-HD dataset, which includes brief videos of people doing Tai-chi exercises, was used for training and evaluation. Following (Siarohin et al., 2020), 3,141 Tai-chi videos were downloaded from YouTube. The videos were cropped and resized to a resolution of  $256^2$ , while the aspect ratio was preserved. There are 3,016 training videos and 125 evaluation videos.

### 4.2. Comparison with Previous Works

In order to compare our work to previous works (Table 4) we used metrics previously used in similar papers. Average Key-points Distance (Cao et al., 2017) (AKD) measures the average key-points distance between the generated video and the source video. Average Euclidean Distance (Zheng et al., 2019) (AED) measures the average euclidean distance between the representations of the ground-truth and generated videos in some embedding space. In addition, we added the L1 distance as well. Our AED and AKD metrics were calculated using the following repository: <https://github.com/AliaksandrSiarohin/pose-evaluation>

Note that those metrics aren't optimal since one can easily improve reconstruction by increasing the bottleneck, and we can see our artifacts in animation results (Table 2). However, our pose did follow the driving video well, and to improve

Table 3. Images comparison 2

SOURCE IMAGE	DRIVING
X2FACE	
MONKEY-NET	
FOMM	
OURS	
OURS (SOFT-MAX)	

Table 4. Accuracy Metrics

METHOD	AKD	AED	L1
X2FACE	17.654	0.272	0.080
MONKEY-NET	10.798	0.228	0.077
FOMM	6.872	0.167	0.063
PERTURBED MASK	4.239	0.147	0.047
OURS (CIRCLES MASK)	14.760	0.245	0.077
OURS	5.551	0.141	0.045
IMPROVEMENT (FOMM)	19.2%	15.5%	28.5%

the identity and background artifacts, we suggest some fixes in Section 5.

## 5. Future work

We would like to test our module on more datasets, and compare them to the state of the art. In addition, summing the heatmap channels might not be optimal, and there is certainly some space to try something deeper with the features extracted in the keypoint detector as an input, or feed all of the channels separately into the generator. We want to experiment with mask thresholds due to the distortions in the animation background. We may also increase the number of keypoints, but that would probably be more beneficent to the second type of mask, and would increase the required GPU memory proportionally. We also thought about coloring matching keypoints with the same color to help the module to learn a motion flow.

## 6. Conclusions

We constructed a novel method for image animation by moving the need for a strong motion prior (optical flow) to the assumption of a pre-trained keypoint detector/keypoint

heatmaps prior to activation, which might be based on a motion prior. By doing so, we encapsulated motion to a motion mask, which is bottlenecked by the prior training which has the keypoint bottleneck. The motion masks are then fed into a generator, which combines the appearance of the source image and the mask which represents the structure, decoupled from any appearance naturally by the assumption that during the training of the keypoint detector, the heatmap mask went into a keypoint bottleneck. After evaluation, we can conclude that our method is feasible, although with some artifacts.

## Software and Data

Detailed in our repository:

<https://github.com/or-toledano/animation-with-keypoint-mask>

## References

- Balakrishnan, G., Zhao, A., Dalca, A. V., Durand, F., and Guttag, J. Synthesizing images of humans in unseen poses. In *Proceedings of the IEEE Conference on Computer Vision and Pattern Recognition*, pp. 8340–8348, 2018.
- Bregler, C., Covell, M., and Slaney, M. Video rewrite: Driving visual speech with audio. In *Proceedings of the 24th annual conference on Computer graphics and interactive techniques*, pp. 353–360, 1997.
- Cao, Z., Simon, T., Wei, S.-E., and Sheikh, Y. Realtime multi-person 2d pose estimation using part affinity fields. In *The IEEE Conference on Computer Vision and Pattern Recognition (CVPR)*, 2017.
- Cheung, G. K., Baker, S., Hodgins, J., and Kanade, T. Markerless human motion transfer. In *Proceedings. 2nd International Symposium on 3D Data Processing, Visualization and Transmission, 2004. 3DPVT 2004.*, pp. 373–378. IEEE, 2004.
- He, K., Zhang, X., Ren, S., and Sun, J. Deep residual learning for image recognition, 2015.
- Kim, Y., Nam, S., Cho, I., and Kim, S. J. Unsupervised keypoint learning for guiding class-conditional video prediction. *arXiv preprint arXiv:1910.02027*, 2019.
- Ma, L., Jia, X., Sun, Q., Schiele, B., Tuytelaars, T., and Van Gool, L. Pose guided person image generation. *arXiv preprint arXiv:1705.09368*, 2017.
- Reed, S., Oord, A., Kalchbrenner, N., Colmenarejo, S. G., Wang, Z., Chen, Y., Belov, D., and Freitas, N. Parallel multiscale autoregressive density estimation. In *International Conference on Machine Learning*, pp. 2912–2921. PMLR, 2017.
- Ronneberger, O., Fischer, P., and Brox, T. U-net: Convolutional networks for biomedical image segmentation, 2015.
- Shalev, Y. and Wolf, L. Image animation with perturbed masks, 2020.
- Siarohin, A., Lathuilière, S., Tulyakov, S., Ricci, E., and Sebe, N. Animating arbitrary objects via deep motion transfer, 2019.
- Siarohin, A., Lathuilière, S., Tulyakov, S., Ricci, E., and Sebe, N. First order motion model for image animation, 2020.
- Simonyan, K. and Zisserman, A. Very deep convolutional networks for large-scale image recognition, 2015.
- Tulyakov, S., Liu, M.-Y., Yang, X., and Kautz, J. Mocogan: Decomposing motion and content for video generation. In *Proceedings of the IEEE conference on computer vision and pattern recognition*, pp. 1526–1535, 2018.
- Wang, T.-C., Liu, M.-Y., Zhu, J.-Y., Liu, G., Tao, A., Kautz, J., and Catanzaro, B. Video-to-video synthesis, 2018.
- Wu, W., Cao, K., Li, C., Qian, C., and Loy, C. C. Transgaga: Geometry-aware unsupervised image-to-image translation, 2019.
- Zheng, Z., Yang, X., Yu, Z., Zheng, L., Yang, Y., and Kautz, J. Joint discriminative and generative learning for person re-identification. *IEEE Conference on Computer Vision and Pattern Recognition (CVPR)*, 2019.